Part One
Molecular Separation

This Part will be focused on the fundamentals and applications of membranes and membrane operations for separation at the molecular level. Both liquid (including organic solvents) and gaseous streams will be discussed.

The book opens with a chapter on molecular modeling to highlight the powerful instruments for designing appropriate membrane materials with predicted properties.

This is followed by a chapter on polymeric membranes that discusses the current achievements and challenges on membranes for molecular separation in liquid phase.

Subsequent individual chapters discuss membranes in organic solvent separation, gas separation and electrochemical separation. A whole chapter is focused on the fundamentals of fouling molecular separation by membranes are completed by a chapter focused on fouling. and another on energy and environmental issues.

The application part of this section illustrates the membrane-assisted molecular separation in (i) gases, with a separate chapter dedicated to the CO_2 capture using inorganic membrane; (ii) water desalination; (iii) downstream processing of biological products. A chapter on integrated membrane operations illustrates new strategies in water treatment and chemical production.

Membrane separation in the medical field has been included in a chapter focused on medical extracorporeal devices, which illustrates the use of membranes for separation of biological fluids and for preparation of bioartificial organs able to accomplish *ex vivo* biological transformation (Part headed 'Transformation').

The overall aim of the 'molecular separation' section is to illustrate the current capability of membranes and membrane operations in assisting and governing molecular separations and the future perspectives they offer for a more sustainable industrial growth through innovative process design. Their implementation will lead to concrete benefits in manufacturing and processing, substantially shrinking equipment size, boosting plant efficiency, saving energy, reducing capital costs, minimizing environmental impact, and using remote control and automation.

Membrane Operations. Innovative Separations and Transformations. Edited by Enrico Drioli and Lidietta Giorno

ISBN: 978-3-527-32038-7

Membrane operations have the potential to replace conventional energy-intensive separation techniques, such as distillation and evaporation, to accomplish the selective and efficient transport of specific components, to improve the performance of reactive processes and, ultimately, to provide reliable options for a sustainable industrial growth.

This is in line with the strategy of process intensification and it is expected to bring substantial improvements in chemical and many other manufacturing and processing industries.

Many membrane operations are based on similar materials and structures, while differing in the method by which they carry out the separation process. Step forward innovations can be promoted by appropriate integration of traditional membrane operations (reverse osmosis, micro-, ultra- and nanofiltration, electrodialysis, pervaporation, etc.) among them and with innovative membrane operations. In fact, while being already widely used in many different applications, they can be combined with new membrane systems such as catalytic membrane reactors and membrane contactors. Nowadays, redesign of industrial production cycles by combining various membrane operations suitable for separation, conversion and concentration units is an attractive opportunity because of the synergic effects that highly integrated membrane processes can promote.

1
Molecular Modeling, A Tool for the Knowledge-Based Design of Polymer-Based Membrane Materials

Dieter Hofmann and Elena Tocci

1.1
Introduction

Most important macroscopic transport properties (i.e., permeabilities, solubilities, constants of diffusion) of polymer-based membranes have their foundation in microscopic features (e.g., free-volume distribution, segmental dynamics, distribution of polar groups, etc.) which are not sufficiently accessible to experimental characterization. Here, the simulation of reasonably equilibrated and validated atomistic models provides great opportunities to gain a deeper insight into these microscopic features that in turn will help to develop more knowledge-based approaches in membrane development.

The mentioned transport properties for small and medium-sized molecules in polymers are decisive in many technologically important processes, for example, in biotechnology and biomedicine, in pharmacological and chemical industries but also in integrated environmental protection. The respective penetrants can be anything from rather small hydrogen or oxygen molecules to chemicals like benzene up to relatively large drug molecules.

Membrane processes for the separation of gaseous and liquid mixtures are important examples. In these cases there are already large numbers of applicable materials and processes. Further improvements (mostly concerning better selectivities at acceptably high permeabilities), often needing real jumps in performance, are, however, still needed in many cases. This applies, although in the opposite sense, also to barrier materials where permeations at least of certain types of molecules will be extremely small. Other areas concern biomaterials or material systems for the controlled release of drugs.

More specific examples for the need to develop new materials with tailored transport properties are:

- The separation of methane from higher hydrocarbons in natural gas for safer and more economical transport through pipelines, or for better exploitation;

Membrane Operations. Innovative Separations and Transformations. Edited by Enrico Drioli and Lidietta Giorno

ISBN: 978-3-527-32038-7

- The design of packaging materials for conservation of fresh fruits and vegetables, which means good specific permeation and selectivity properties in order to maintain a modified/controlled atmosphere;
- The control of migration of additives, monomers or oligomers, from packaging materials, for example, into food (important for the enforcement of a high level of food quality and safety) or other consumer products;
- The resistance of resins used in composites for aircraft construction to ageing caused by water absorption;
- Small but continuous fuel loss by permeation through polymeric parts of the fuel system;
- Separation of CO_2 from flue gases, and separation of NO_x from vehicle emissions;
- Efficient and inexpensive proton-conducting membranes for fuel cells;
- components in polymer electronics (such as for light-emitting diodes or display components) with extremely low permeabilities for oxygen and water;
- Optimum controlled drug release systems, for example, for medical applications, cosmetics or agriculture;
- Transport problems in artificial or bio-hybrid organs;
- Optimum biocompatibility of polymers in contact with cells and blood;
- Optimum chemical degradation behavior (often to a large extent a water-permeation problem) for surgical sutures, scaffold materials for tissue engineering, degradable screws in orthopaedic surgery and so on.

In the near future, the use of multifunctional polymer-based materials with separation/selective transport capabilities is also to be expected in the design of production systems with integrated environmental protection or in the combination of chemical reactions and separation by attaching a catalytic functionality to the respective material [1]. Thus, those multifunctional materials should contribute materially to the development of clean energy and/or energy saving and therefore sustainable production technologies. In connection with these perspectives, there is considerable interest in new/modified polymer-based materials with tailored transport/catalytic properties. Also, many sensor applications are based on controlled permeation.

Amorphous polymers or respective composites with inorganic components are an important class of materials to solve many of the above-mentioned problems. However, the design of these multifunctional materials, based on experimentation and correlative thinking alone is unreliable, time consuming, expensive and often not successful. Systematic multiscale computer-aided molecular design (CAMD) offers a very attractive alternative, insofar as these techniques allow for the very elaborate investigation of complex material behavior with regard to the links between structure, dynamics and relevant properties of the discussed multifunctional polymer-based materials on the length and time scales (from Angstroms to micrometers and from picoseconds to milliseconds, respectively) which are most important for the penetrant transport and other relevant processes (e.g., selective transport, separation, catalysis, biodegradation, sensor applications) of interest. In the present chapter, molecular modeling tools (i.e., quantum chemistry (QM), atomistic- and mesoscale modeling) will be in the focus of interest. Consequently, the microscopic properties to

be related with macroscopically determined transport parameters are, for example, chain stiffness parameters, free volume and its distribution, mobility measures for chain segments, energy densities describing interactions of chain segments with penetrants, microscopic effects of swelling and so on.

Over the last 15 years particularly atomistic molecular modeling methods have found widespread application in the investigation of small-molecule permeation [2–15].

1.2 Basics of Molecular Modeling of Polymer-Based Membrane Materials

The permeation of small molecules in amorphous polymers is typically following the solution diffusion model, that is, the permeability P_i of a feed component i can be envisioned as the product of the respective solubility S_i and constant of diffusion D_i. Both parameters can be obtained experimentally and in principle also by atomistic simulations.

The molecular modeling of these polymers typically starts with the construction of normally rectangular packing models. There, the related chain segments of the respective polymer will be arranged in realistic, that is, statistically possible, way. To do this, first the involved atoms are considered to be spheres of the respective atomic radius R_i (as obtainable from QM) and atomic weight m_i. The bonded interactions between atoms resulting in bonds, bond angles and conformation angles are then described by mechanic springs or torsion rods with spring constants related to, for example, experimentally known bond strengths. So-called nonbond interactions between atoms that either belong to different molecules or that in one and the same molecule are further apart from each other than about three bonds are considered via, for example, Lennard-Jones (to describe van der Waals interactions) and Coulomb potentials (to describe electrostatic interactions). The sum of all interatomic interactions written as the potential energy of a packing model is then called a forcefield. Forcefields form the core of all atomistic molecular modeling programs. Equation 1.1 shows the principal structure of a typical forcefield for a system of N atoms with the Cartesian atomic position vectors $\vec{r}_i$.

$$\begin{aligned} V(\vec{r}_1, \vec{r}_2, \ldots, \vec{r}_N) = & \sum_{\text{Covalent bonds}} K_b (l - l_0)^2 + \sum_{\text{Bond angles}} K_\Theta (\Theta - \Theta_0)^2 \\ & + \sum_{\text{Dihedral angles}} K_\varphi [1 + \cos(n\varphi - \delta)] \\ & + \sum_{\text{nonbonded atom pairs } i,j} \left[\left(\frac{a_{ij}}{r_{ij}^{12}} \right) - \left(\frac{b_{ij}}{r_{ij}^{6}} \right) + \frac{q_i q_j}{\varepsilon_0 \varepsilon_r r_{ij}} \right] \end{aligned} \tag{1.1}$$

with the following parameters:

l = actual length of a bond
l_0 = length of a bond in equilibrium
K_b = force constant for a bond length deformation
Θ = actual value for a bond angle
Θ_0 = value for a bond angle in equilibrium
K_Θ = force constant for a bond-angle deformation
φ = actual value for a conformation angle
n = periodicity parameter in a conformation potential
δ = constant to fix trans-state in a conformation potential
K_φ = force constant for a conformation potential
R_{ij} = distance between atoms i and j with $(j - i) > 3$
a_{ij} = constant describing repulsive interactions in the *Lennard-Jones* Potential
b_{ij} = constant describing attractive interactions in the *Lennard-Jones* Potential
q_i = partial charge of the ith atom
ε_0 = vacuum permittivity
ε_r = dielectric constant.

The parameters l_0, K_b, Θ_0, K_Θ, K_φ, n, δ, a_{ij}, b_{ij}, q_i, q_j and ε_r belong to the fit parameters, which can be determined by fitting of Equation 1.1 to a sufficient set of data calculated by QM and/or determined experimentally (e.g., X-ray scattering, IR spectroscopy, heats of formation). From a numeric point of view the pair interaction terms (van der Waals and Coulomb) are most demanding. In this connection the typical size of polymer packing models is limited to typically 3000–10 000 atoms (leading to lateral sizes of bulk models of a few nm), although in other connections now also models with up to 100 000 atoms have been used.

Forcefields may be utilized in two directions:

Model systems can be, on the one hand, subjected to a static structure optimization. There, the fact is considered that the potential energy of a relaxed atomistic system (cf. Equation 1.1) should show a minimum value. Static optimization then means that by suited numeric procedures the geometry of the simulated system is changed as long as the potential energy reaches the next minimum value [16]. In the context of amorphous packing models, the main application for this kind of procedure is the reduction of unrealistic local tensions in a model as a prerequisite for later molecular dynamic (MD) simulations.

It is, on the other hand, possible to use the potential energy of a model system as described by Equation 1.1 to calculate the forces $\vec{F}_i$ acting on each atom of the model via the gradient operation:

$$\vec{F}_i = -\frac{\partial V(\vec{r}_1, \vec{r}_2, \ldots, \vec{r}_N)}{\partial \vec{r}_i} \tag{1.2}$$

Then, Newton's equations of motion can be solved for every atom of the investigated system:

$$\vec{F}_i = m_i \frac{d^2 \vec{r}_i(t)}{dt^2} \tag{1.3}$$

The necessary starting positions $\vec{r}_i(0)$of the atoms are in the given case usually obtained from methods of chain-packing procedures (see below). The starting velocities $\vec{v}_i(0)$ of all atoms are assigned via a suited application of the well-known relation between the average kinetic E_{kin} energy of a polyatomic system and its temperature T:

$$E_{kin} = \sum_{i=1}^{N} \frac{1}{2} m_i \vec{v}_i^{\,2} = \frac{3N-6}{2} k_b T \tag{1.4}$$

k_B is the Boltzmann constant. $(3N-6)$ is the number of degrees of freedom of an N-atom model considering the fact that in the given case the center of mass of the whole model with its 6 translation and rotation degrees of freedom does not move during the MD simulation. Using Equations 1.2–1.4 it is then possible to follow, for example, the motions of the atoms of a polymer matrix and the diffusive movement of imbedded small penetrant molecules at a given temperature over a certain interval of time.

Equation 1.3 represents a system of usually several thousand coupled differential equations of second order. It can be solved only numerically in small time steps Δt via finite-difference methods [16]. There always the situation at $t + \Delta t$ is calculated from the situation at t. Considering the very fast oscillations of covalent bonds, Δt must not be longer than about 1 fs to avoid numerical breakdown connected with problems with energy conservation. This condition imposes a limit of the typical maximum simulation time that for the above-mentioned system sizes is of the order of several ns. The limited possible size of atomistic polymer packing models (cf. above) together with this simulation time limitation also set certain limits for the structures and processes that can be reasonably simulated. Furthermore, the limited model size demands the application of periodic boundary conditions to avoid extreme surface effects.

The already mentioned limited lateral dimensions of packing models of just several nm makes it impossible to simulate complete membranes or other polymer-based samples. Therefore, on the one hand, bulk models are considered that are typically cubic volume elements of a few nanometers side length that represent a part cut out of the interior of a polymer membrane (cf. Figure 1.1). On the other hand interface models are utilized, for example, for the interface between a liquid feed mixture and a membrane surface or between a membrane surface and an inorganic filler (cf. Figure 1.2).

1.3 Selected Applications

1.3.1 Hard- and Software

The InsightII/MaterialsStudio/Discover software of Accelrys [18, 19] was utilized for the amorphous packing model construction, equilibration and the atomistic

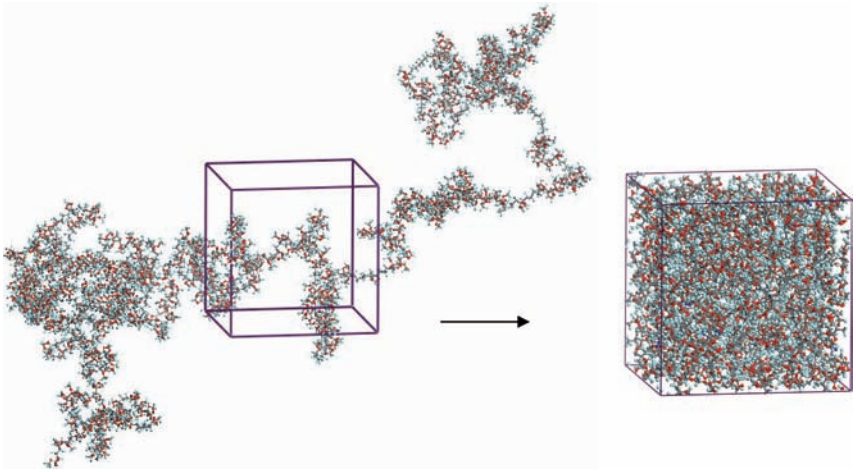

Figure 1.1 Atomic representation of a typical 3-dimensional packing model (thickness about 3 Å) starting with a single Hyflon AD60X polymer chain. Atom colors: gray = carbon, red = oxygen, light blue = fluorine [15].

simulations. In most of the following examples the COMPASS forcefield was applied [20, 21].

For data evaluation also self-programmed software (mostly in BTCL, Fortran, C) was applied. Data production runs were performed on a 74 processor Opteron Linux Cluster, a SGI Origin 2100 and on SGI Onyx workstation.

1.3.2 Simulation/Prediction of Transport Parameters and Model Validation

The quality of atomistic packing models is typically validated via comparisons between measured and simulated properties like wide-angle X-ray scattering (WAXS)

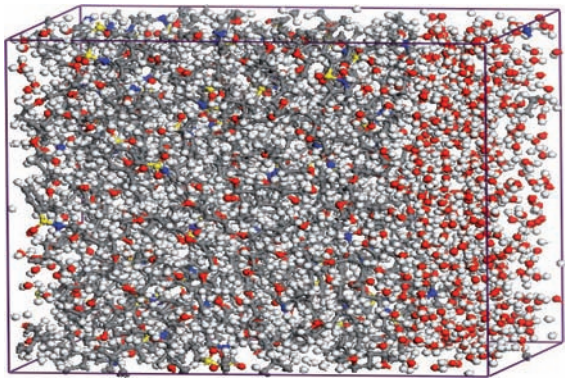

Figure 1.2 Atomic representation of a surface model of Pebax/30%KET with water [17].

curves, densities, transport parameters for small and medium sized penetrants. In the latter case both validating (if a polymer is already existing and experimentally characterized) and predictive (if a polymer has not been synthesized yet or if no transport parameters are available experimentally) applications are possible.

1.3.2.1 Prediction of Solubility Parameters

Here, hitherto in most cases the transition-state method of Gusev and Suter [22, 23] was utilized to first determine calculated solubility values S_{calc} values. There, a fine 3D-grid with a grid spacing of about 0.03 nm is layered over a completely refined detailed-atomistic amorphous polymer bulk packing model (cf. Figure 1.1). Then a small virtual test molecule of the intended kind (e.g., O_2) in a united atom representation is inserted in the polymer matrix at each lattice point of the grid. The resulting nonbonded interaction energy E_{ins} between the inserted molecule and the whole polymer matrix is calculated for each position of the respective inserted molecule. Only the van der Waals interactions are considered, that is, the method would not work for highly polar penetrants like water. Furthermore, since the polymer matrix can not locally relax to accommodate larger inserted penetrants it only works for small molecules (typically just up to O_2, N_2, etc.). From the insertion energy data via Equation 1.5 the chemical excess potential μ_{ex} for infinite dilution can be calculated and converted in the respective solubility using Equation 1.6.

$$\mu_{ex} = RT \times \ln < \exp(-E_{ins}/kT) > \tag{1.5}$$

$$S_{calc} = \frac{T_0}{p_0 T} \exp\left(-\frac{\mu_{ex}}{kT}\right) \tag{1.6}$$

with R being the universal gas constant and T_0 and p_0 being temperature and pressure under standard conditions ($T_0 = 273.15$ K; $p_0 = 1013 \times 10^5$ Pa).

Table 1.1 contains typical solubility prediction data for an ultrahigh free-volume polymer (PTMSP) and a polymer with more conventional transport properties (PTMSS).

As already mentioned the Gusev–Suter method normally only works for small penetrant molecules like oxygen or nitrogen. For a long time no really generally applicable alternative method was available to overcome the problem, but a few years ago Boulougouris, Economou Theodorou *et al.* [27, 28] suggested a new inverse Widom method based on the particle-deletion algorithm "DPD" to overcome this problem in principle. The related computer code was, however, only applicable to special, relatively simple model systems. Based on DPD also a generalized version of this algorithm was presented in the literature [29] permitting the calculation of solubility coefficients for molecules as large as, for example, benzene in polymers for which reasonable forcefield parameters exist. Table 1.2 contains solubility data for a number of penetrants of different size in PDMS obtained in this way.

1.3.2.2 Prediction of Diffusion Constants

The following description again follows the already quoted papers of Gusev and Suter. Using the E_{ins} values mentioned in the foregoing section, the whole packing model in

Table 1.1 Results of application of the Gusev–Suter method to the solubility of N_2 in PTMSP and PTMSS.

Polymer	Structure formula	Average simulated N_2 solubility coefficient S_{calc} [cm^3(STP)/(cm^3 atm)]	Average measured N_2 solubility coefficient S_{exp} [cm^3(STP)/(cm^3 atm)]
PTMSP	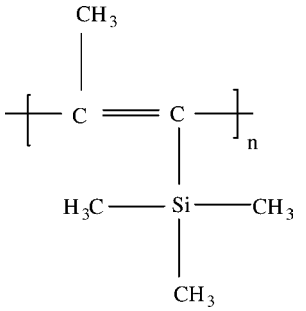	1.16 [24]	1.02 [25]
PTMSS	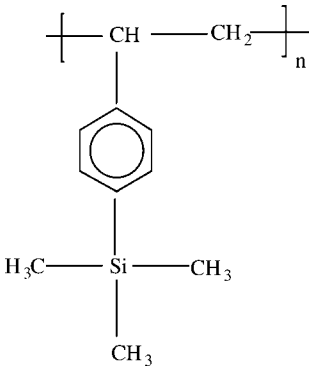	0.19 [24]	0.18 [26]

question is separated into regions of free volume (low interaction energy) and regions of densely packed polymer (high interaction energy; cf. Figure 1.3). The borders between the energetically attractive regions $E_{ins}(x, y, z)$ around the resulting local insertion energy minima are given as crest surfaces of locally maximum insertion energy. In the two-dimensional analogy of a cratered landscape a minimum energy region would be represented by a crater, while the crest surface of locally maximum insertion energy would be reduced to the crest line separating one crater from the adjacent ones. From this identification of energetically separated sites where a penetrant would typically sit (approximately the centers of holes) and jump probabilities between adjacent sites (which can be calculated by proper integration over the mentioned crest lines and "craters" of the insertion energy function $E_{ins}(x, y, z)$ an efficient Monte Carlo simulation method for the jump-like diffusion of small

Table 1.2 Results of application of a generalized DPD method to different penetrants in PDMS.

Solute	S_{calc} [cm^3(STP) cm^{-3} bar^{-1}]	S_{exp} [cm^3(STP) cm^{-3} bar^{-1}]
Oxygen	0.32[a]	0.224[b]
Nitrogen	0.13[a]	0.127[b]
Acetone	69[a]	33–66[c]
Benzene	495[a]	275–624[d]

[a][29, 30].
[b][31].
[c][32].
[d][33].

molecules in a polymer matrix can be developed (cf. Figure 1.4). With this algorithm the simulation range can almost extend in the ms range. That is, in most cases the normal diffusive regime can be reached and the respective constant of diffusion D_i can be obtained via the Einstein equation from the slope of the mean squared displacement $s_i(t)$:

$$\vec{s}_i(t) = \langle |\vec{r}_i(t) - \vec{r}_i(0)|^2 \rangle \tag{1.7}$$

$$\rightarrow D_i(t) = \frac{\langle |\vec{r}_i(t) - \vec{r}_i(0)|^2 \rangle}{6t} \tag{1.8}$$

Here, $\vec{r}_i(t)$is the position vector of penetrant i and <> is the average over all possible time origins $t = 0$ and all simulated trajectories of a penetrant of a given kind. Again, as with the solubilities the Gusev–Suter method can only handle small penetrants in this way, because the respective polymer matrix cannot conformationally adjust to larger penetrants. Table 1.3 contains a comparison between experimental and

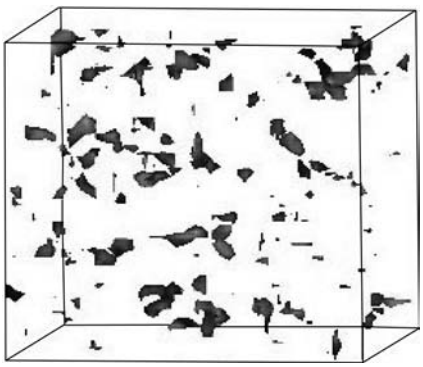

Figure 1.3 Free volume for a perfluorinated polymer in red indicating into the densely packed polymer.

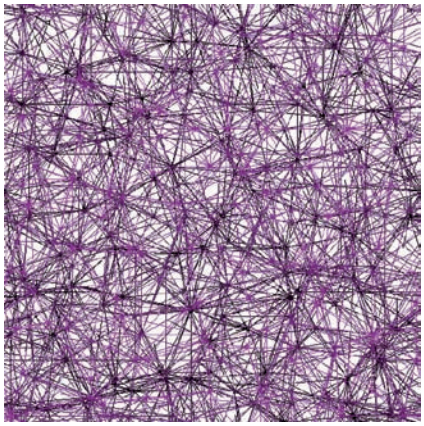

Figure 1.4 Jump-like diffusion of oxygen molecules in a perfluorinated polymer matrix.

calculated values, D_{exp} and D_{calc}, respectively for a number of gases in PTMSP. Here, for methane and carbon dioxide it has to be considered that these molecules are normally already too large to lead to reasonable results with the Gusev–Suter method.

In comparing simulated and experimentally measured transport parameters one has to be aware that experimental data in the literature depending, for example, on sample preparation conditions and the chosen measurement methodology can show a considerable scatter, often reaching a factor of two or even more. It is, for example well-known that polyimides often contain residual solvent filling a part of the free volume and thus leading to systematically lower S and D values from experiments than from simulations [34].

1.3.3
Permeability of Small Molecules and Free-Volume Distribution

The distribution of free volume in amorphous polymers is of paramount importance for the respective material's transport behavior towards small and medium-sized penetrants.

Table 1.3 Results of application of the Gusev–Suter method for the diffusion constants of different penetrants in PTMSP.

Solute	D_{calc} [10^{-5} cm^2/s]	D_{exp} [10^{-5} cm^2/s]
Nitrogen	7.7[a]	3.50[b]
Oxygen	7.5[a]	4.66[b]
Methane	8.2[a]	2.64[b]
Carbon dioxide	9.2[a]	8.02[b]

[a][24].
[b][25].

While in rubbery polymers differences in the segmental mobility can be more important than differences in the free-volume distribution for glassy polymers often certain basic correlations can be found between the permeability of small molecules and free-volume distribution. Other important factors are the molecular mobility of chain segments and the local chemical composition.

Experimentally, the free-volume distribution can be best characterized with positron annihilation lifetime spectroscopy (PALS). There, in organic glasses ortho-positronium (o-Ps) which has a lifetime of 142 ns in vacuo shows a strong tendency to localize in heterogeneous regions of low electron density (holes). In polymeric materials the vacuum lifetime is cut short via the "pick-off" mechanism, where o-Ps prematurely annihilates with one of the surrounding bound electrons. This lifetime can (under certain assumptions) be converted in an average hole radius [35, 36], while the intensity of the lifetime signal may permit conclusions about the overall contents of free volume. There are, however, a number of shortcomings with common PALS methodology. Often, the holes forming the free volume are assumed to be just spheres and the shape of calculated hole radius distribution peaks is set to Gaussian. Furthermore, positrons in their limited lifetime seem not to be capable of probing large holes of complex topology (cf. in particular PTMSP and other ultrahigh free-volume polymers) [24, 37]. Finally the size of the positronium molecule does only permit probing of the accessible free volume for molecules about the size of hydrogen.

Atomistic molecular modeling utilizing bulk models on the other hand can provide additional even more detailed information about free-volume distributions in amorphous polymers. In this way, glassy polymers, where individual differences in chain segment mobility do not have an as distinct influence on transport properties than in rubbery polymers, can be roughly grouped into three classes regarding their small molecule permeability, as will be outlined in the following for the example of oxygen.

1.3.3.1 Examples of Polymers with Low Permeability of Small Molecules (e.g., $PO_2 \leq 50$ Barrer)

Figure 1.5(a) shows as a typical example a computer-tomography-like atomic monolayer representation of a bulk model for diisopropyldimethyl PEEK WC (DIDM-PEEK). In this case the oxygen-accessible free volume is obviously organized in relatively small isolated holes and the respective size distribution (cf. Figure 1.5(b)) is monomodal and extending only to hole radii of about 5 Å.

1.3.3.2 Examples of Polymers with High Permeability of Small Molecules (e.g., 50 Barrer $\leq PO_2 \leq$ 200 Barrer)

Similarly to Figure 1.5(a), Figure 1.6(a) displays an atomic monolayer representation for a so-called high-performance polymer (here PPrSiDPA with a PO_2 of 230 Barrer [38]). Already in this view larger holes are visible than for the case of low-performance polymers (cf. Figure 1.5(a)) and the hole-size distribution (Figure 1.6(b)) reveals a much wider range of radii (here extending to 10 Å and being bi-modal). This situation is quite typical for polymers with high gas transport capacity. A more systematic study

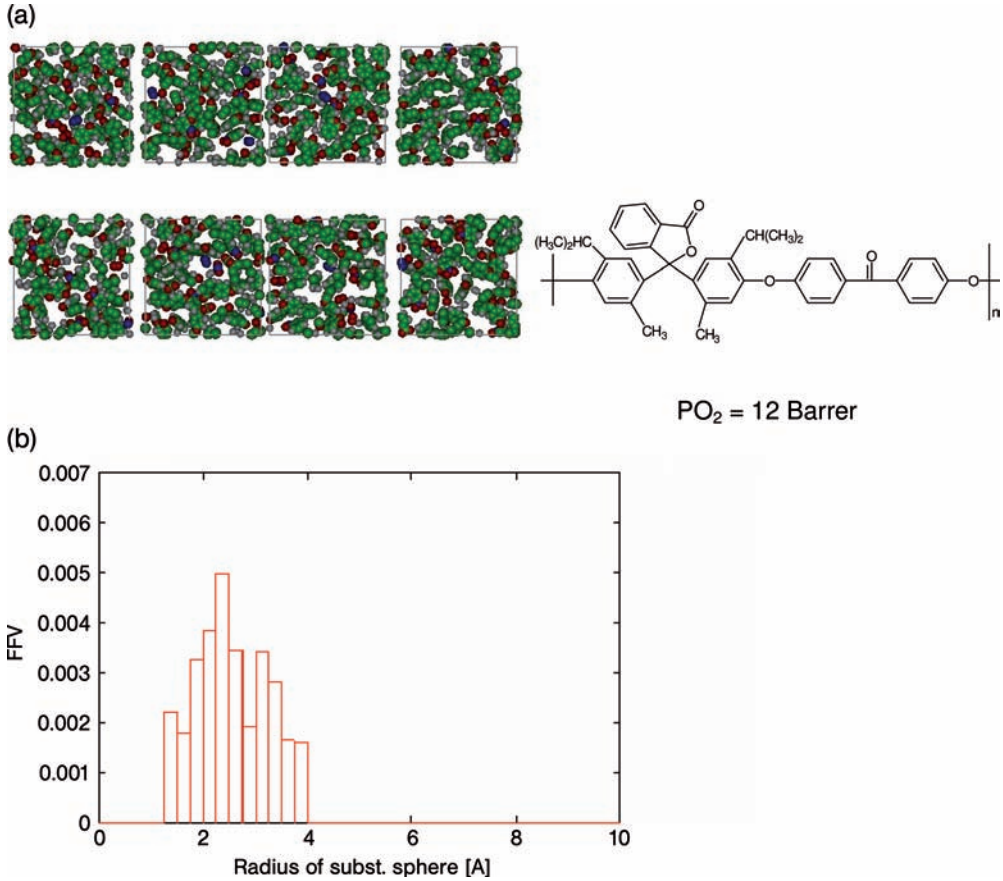

Figure 1.5 (a) Atomic monolayer representation (thickness about 3 Å) of a typical packing model and structure formula for DIDMPEEK. (b) Hole-size distribution for the packing model shown in Figure 1.5(a).

on polyimides [34] did, for example, reveal that the major difference between low-performance and high-performance polyimides with about the same overall contents of free volume lies in the distribution of the (e.g., oxygen) accessible free volume. Low-performance polyimides show just a monomodal distribution extending up to about 5 Å, while high-performance polyimides behave more or less similar to the example illustrated in Figure 1.6.

1.3.3.3 Examples of Polymers with Ultrahigh Permeability of Small Molecules (e.g., $PO_2 \geq 1000$ Barrer)

Figure 1.7 then shows respective data for an ultrahigh free-volume and performance polymer, Teflon AF2400 of DuPont ($PO_2 = 1140$ Barrer; [39]). One can recognize that

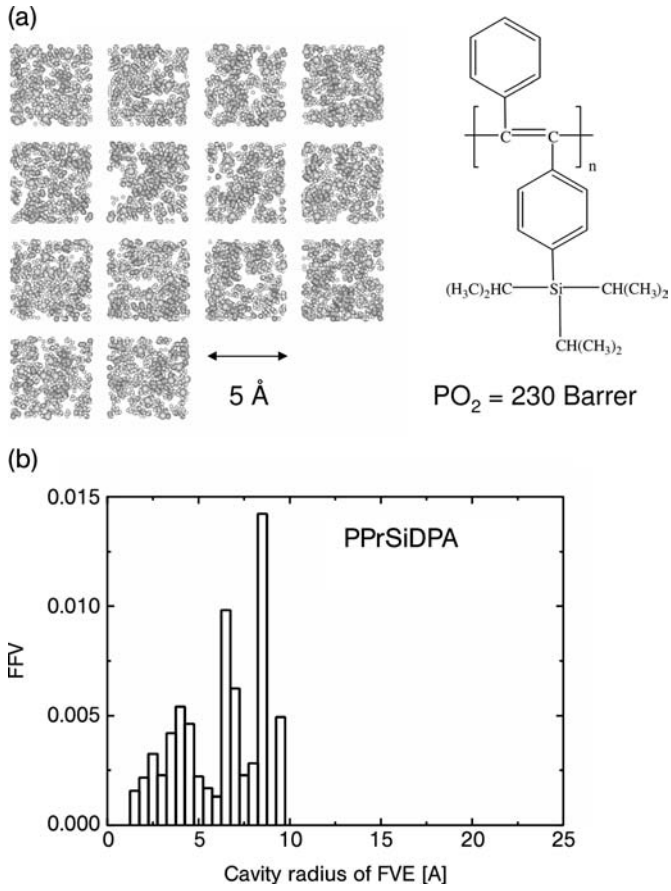

Figure 1.6 (a) Atomic monolayer representation (thickness about 3 Å) of a typical packing model and structure formula for PPrSiDPA. (b) Hole-size distribution for the packing model shown in Figure 1.6(a).

in this case there is "conventional" free volume organized in isolated holes in the radius range below 10 Å existing in parallel with a partly continuous phase of much larger holes that in this case are visible as a peak between 15 and 20 Å. The effect is even more pronounced for PTMSP, the polymer of this kind with the highest oxygen permeability so far measured (about 9000 Barrer; [38]). There, the continuity for the large-hole phase is more clearly visible already in atomic monolayer representations of respective packing models [37] and the ratio between the area under the "conventional" free-volume peak and the continuous hole phase peak in the hole-size distribution is even smaller than for Teflon AF2400.

The fact that for the mentioned ultrahigh free-volume polymers the continuous hole-phase peak appears at rather limited values is related with the limited size of the

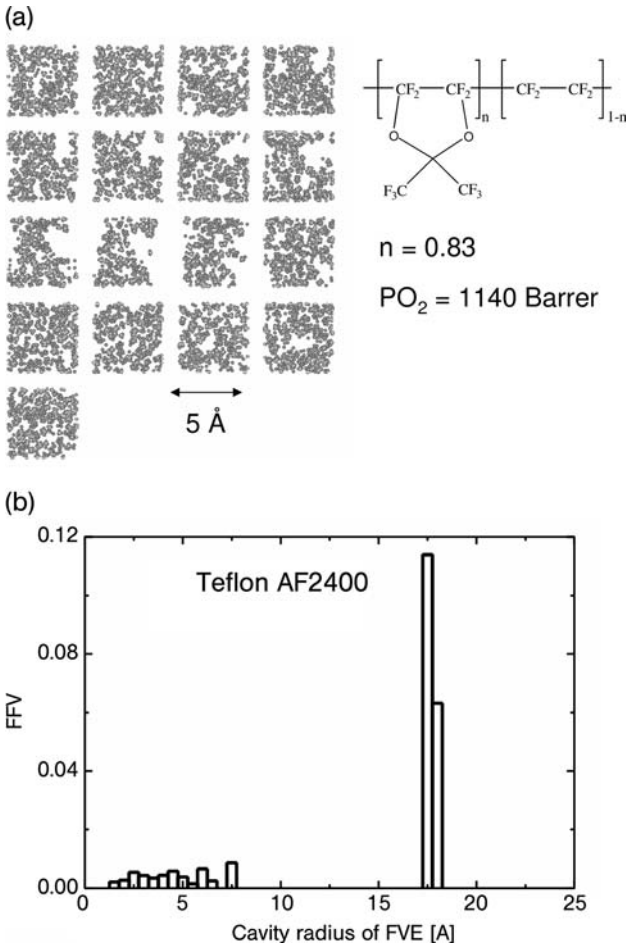

Figure 1.7 (a) Atomic monolayer representation of a typical packing model and structure formula for Teflon AF2400. (b) Hole-size distribution for the packing model shown in Figure 1.7(a).

investigated models (45–50 Å) while the thickness of real polymer membranes can extend into the micrometer range.

1.4 Summary

Atomistic molecular modeling techniques have proven to be a very useful tool for the investigation of the structure and dynamics of dense amorphous membrane polymers and of transport processes in these materials. By utilizing these methods, information can be obtained that is not accessible by experimental means.

Acknowledgments

The work was in part supported by the European projects "Growth" Program, "PERMOD – Molecular modeling for the competitive molecular design of polymer materials with controlled permeability properties." Contract #G5RD-CT-2000-200, the 6 Framework Programme project "MULTIMATDESIGN- Computer aided molecular design of multifunctional materials with controlled permeability properties", Contract no.: 013644, INTAS - RFBR 97–1525 grant.

References

1 Drioli, E., Natoli, M., Koter, I. and Trotta, F. (1995) *Biotechnology and Bioengineering*, **46**, 415.

2 Boyd, R.H. and Krishna Pant, P.V. (1991) *Macromolecules*, **24**, 6325.

3 Müller-Plathe, F. (1991) *Journal of Chemical Physics*, **94**, 3192.

4 Sok, R.M., Berendsen, H.J.B. and van Gunsteren, W.F. (1992) *Journal of Chemical Physics*, **96**, 4699.

5 Krishna Pant, P.V. and Boyd, R.H. (1993) *Macromolecules*, **26**, 679.

6 Gusev, A.A., Müller-Plathe, F., van Gunsteren, W.F. and Suter, U.W. (1994) *Advances in Polymer Science*, **16**, 207.

7 Tamai, Y., Tanaka, H. and Nakanishi, K. (1994) *Macromolecules*, **27**, 4498.

8 Chassapis, C.S., Petrou, J.K., Petropoulos, J.H. and Theodorou, D.N. (1996) *Macromolecules*, **29**, 3615.

9 Fried, J.R., Sadad-Akhavi, M. and Mark, J.E. (1998) *Journal of Membrane Science*, **149**, 115.

10 van der Vegt, N.F.A., Briels, W.J., Wessling, M. and Strathmann, H. (1999) *Journal of Chemical Physics*, **110**, 11061.

11 Hofmann, D., Fritz, L., Ulbrich, J., Schepers, C. and Böhning, M. (2000) *Macromolecular Theory and Simulations*, **9**, 293.

12 Tocci, E., Hofmann, D., Paul, D., Russo, N. and Drioli, E. (2001) *Polymer*, **42**, 521.

13 Neyertz, S. and Brown, D. (2001) *Journal of Chemical Physics*, **115**, 708; Neyertz, S. Brown, D. Douanne, A. Bas, C. and Albérola, N.D. (2002) *The Journal of Physical Chemistry. B*, **106**, 4617.

14 van der Vegt, N.F.A. (2002) *Journal of Membrane Science*, **205**, 125; van Gunsteren, W.F. and Berendsen, H.J.C. (1990) *Angewandte Chemie*, **29**, 992.

15 Macchione, M., Jansen, J.C., De Luca, G., Tocci, E., Longeri, M. and Drioli, E. (2007) *Polymer*, **48**, 2619–2635.

16 Haile, J.M. (1992) *Molecular Dynamics Simulation Elementary Methods*, Wiley Interscience, New York.

17 Tocci, E., Gugliuzza, A., De Lorenzo, L. and Drioli, E. in preparation.

18 (1999) *Polymer User Guide, Amorphous Cell Section, Version 400p+*, Molecular Simulations Inc., San Diego, CA.

19 (1999) *Discover User Guide, Polymer User Guide, Amorphous Cell Section, Version 4.0.0p+*, Molecular Simulations Inc., San Diego, CA.

20 Sun, H. and Rigby, D. (1997) *Spectrochim Acta*, **53A**, 1301.

21 Rigby, D. Sun, H. and Eichinger, B.E. (1997) *Polymer International*, **44**, 311.

22 Gusev, A.A. Arizzi, S. and Suter, U.W. (1993) *Journal of Chemical Physics*, **99**, 2221.

23 Gusev, A.A. and Suter, U.W. (1993) *Journal of Chemical Physics*, **99**, 2228.

24 Hofmann, D., Heuchel, M., Yampolskii, Yu., Khotimskii, V. and Shantarovich, V. (2002) *Macromolecules*, **35**, 2129–2140.

25 Ichiraku, Y., Stern, S.A. and Nakagawa, T. (1987) *Journal of Membrane Science*, **34**, 5–18; Masuda, T., Iguchi, Yu., Tang, B.-Z. and Higashimura, T. (1988) *Polymer*, **29**, 2041–2049; Bondar, V.I. (1995) Ph.D.

Thesis, Institute of Petrochemical Synthesis, Moscow.

26 Khotimskii, V.S., Filippova, V.G., Bryantseva, I.S., Bondar, V.I., Shantarovich, V.P. and Yampolskii, Y.P. (2000) *Journal of Applied Polymer Science*, **78**, 1612–1620.

27 Boulougouris, G.C., Economou, I.G. and Theodorou, D.N. (2001) *Journal of Chemical Physics*, **115**, 8231–8237.

28 Boulougouris, G.C., Voutsas, E.C., Economou, I.G., Theodorou, D.N. and Tassios, D.P. (2001) *The Journal of Physical Chemistry B*, **105**, 7792–7798.

29 Siegert, M.R., Heuchel, M. and Hofmann, D. (2007) *Journal of Computational Chemistry*, **28**, 877–889.

30 Simulated data from, Siegert, M.R. (2006) PhD Thesis, Berechnung von Löslichkeitskoeffizienten in Polymer-Materialien, FU-Berlin.

31 Kamiya, Y., Naito, Y., Hirose, T. and Mizoguchi, K. (1990) *Journal of Polymer Science, Part B, Polymer Physics*, **28** (8), 1297–1308.

32 Singh, A., Freeman, B.D. and Pinnau, I. (1998) *Journal of Polymer Science, Part B, Polymer Physics*, **36** (2), 289–301; Frahn, J. (GKSS), personal communication.

33 Summers, W.R., Tewari, Y.B. and Schreiber, H.P. (1972) *Macromolecules*, **5** (1), 12–16; Lichtenthaler, R.N., Liu, D.D. and Prausnitz, J.M. (1974) *Berichte der Bunsen-Gesellschaft — Physical Chemistry Chemical Physics*, **78** (5), 470–477; Grate, J.W., Kaganove, S.N. and Bhethanabotla, V.R. (1997) *Faraday Discussions*, **107**, 259–283; Frahn, J. (GKSS), personal communication.

34 Heuchel, M., Hofmann, D. and Pullumbi, P. (2004) *Macromolecules*, **37**, 201.

35 Gregory, R.B. and Yongkang, Zhu (1991) *Positron and Positron Chemistry* (ed. Y.C. Jean), World Scientific, Singapore, p. 136.

36 Provensher, S.W. (1982) *Computer Physics Communications*, **27**, 229.

37 Hofmann, D., Entrialgo-Castano, M., Lerbret, A., Heuchel, M. and Yampolskii, Yu. (2003) *Macromolecules*, **36**, 8528–8538.

38 Yampolskii, Yu.P., Korikov, A.P., Shantarovich, V.P., Nagai, K., Freeman, B.D., Masuda, T., Teraguchi, M. and Kwak, G. (2001) *Macromolecules*, **34**, 1788–1796.

39 Alentiev, A.Yu., Yampolskii, Yu.P., Shantarovich, V.P., Nemser, S.M. and Platé, N.A. (1997) *Journal of Membrane Science*, **126**, 123–132.